Proceedings Paper:
Herterich, JA, Black, L and Richardson, I (2015) Microstructure and Phase Assemblage of Low-Clinker Cements during Early Stages of Carbonation. In: Black, L and richardson, I, (eds.) The 14th International Congress on the Chemistry of Cement ⬚ICCC 2015⬚Abstract Book Volume 1. International Congress on the Chemistry of Cement (ICCC), 13-16 Oct 2015, Beijing, China. .

Microstructure and Phase Assemblage of Low-Clinker Cements during Early Stages of Carbonation

Julia Herterich[1]*, Black, L.[1], Richardson, I.[1]

1. Institute for Resilient Infrastructure, School of Civil Engineering, University of Leeds, Woodhouse Lane, Leeds LS2 9JT, United Kingdom

Abstract

This study investigates the effects of carbonation following short curing periods (72 hours) on CEMI and composite cement systems (30% PFA, 30% & 60% GGBS). Modifications in carbonation behaviour were observed compared to *'idealised'/28 day lab cured samples and accelerated carbonation testing.* Carbonation of $Ca(OH)_2$ and C-S-H did not occur simultaneously, with decalcification of C-S-H only beginning once no more $Ca(OH)_2$ was available. Decalcification and dealumination of the C-S-H phase occurred following exposure to ambient $[CO_2]$, and $CaCO_3$ microcrystals were observed in the outer product (Op) regions only. A reduction in the Ca/Si ratio of the Ip C-S-H appears to be a result of migration of the Ca ions, driven by a concentration gradient. Furthermore, the rate and extent of carbonation and the nature of the carbonate species formed is dependent on the level of replacement, the replacement material and the degree of hydration. Predominantly calcite was the polymorph formed, however some vaterite was also observed in the samples containing PFA. STA data indicated the production of a crystalline carbonate phase resulting from carbonation of $Ca(OH)_2$ and a metastable, poorly crystalline carbonate phase resulting from the carbonation of the C-S-H phase.

Originality

Though it is well established that a reduced rate of hydration is observed in composite cement materials, both the PC and the SCM will hydrate simultaneously, however there is still a significant lack of knowledge regarding the early age kinetics of the reactions taking place. This becomes of great importance when considering the early removal of formwork in practice, where the reliance is on models established for PC systems. A comprehensive understanding of the complex relationship between slower composite hydration, drying of the sample surface and phase carbonation kinetics is imperative. Current models derived from idealistic, i.e. fully hydrated and non-carbonated, materials, are ineffective for durability predictions. In addition to this, the existing models do not consider the effects that insufficient curing and phase carbonation have on the phase assemblage composition, development of the microstructure and the subsequent consequences for the transport properties. New models relating these factors are crucial for the further development and understanding of service life design. The main objective of this project will be to develop an understanding of the changes and development of the early stage morphology and phase assemblage of composite systems as a result of carbonation, focusing on the changes in carbonation behaviour in composite cement materials following short periods of curing.

Keywords: Early age; Carbonation; Phase assemblage; Morphology

---

[1] Corresponding author: cn08j6h@leeds.ac.uk

1. Introduction

The increasing and widespread use of supplementary cementitious materials (SCMs) in the cement industry has become common practice. The use of such composite cements is valuable in terms of both environmental and engineering aspects, acknowledging the ever rising pressures to further reduce carbon emissions associated with cement manufacture as well as an improvement in material durability through enhancement of the cement microstructure. However, composite cements exhibit reduced rates of hydration, making their improved technological properties dependant on extended periods of moist curing. The need for appropriate curing procedures is recognised in concrete standards where modified curing periods and regimes are recommended in relation to the development of particular properties within the surface region (BS EN 13670:2009). It is also demonstrated extensively throughout the literature (Cakir & Akoz, 2008, Poon et al. 1997), which highlights the amplified adverse effects which inadequate curing methods can have on composite cement materials compared to traditional CEMI systems. Failure to adhere to these prolonged curing guidelines by the early removal of formwork in construction practice may cause fundamental problems in regards to material performance, exposing a microstructure in which hydration is very much incomplete. Consequently, additional information regarding material performance is needed, especially at these very early ages.

Pulverised fuel ash (PFA) and ground granulated blast furnace slag (GGBS) are industrial by-products commonly used as SCMs. Though the reduced rate of hydration is well established, both the Portland cement (PC) and the SCM will hydrate simultaneously, yet there remains a lack of knowledge regarding the early age kinetics of the reactions taking place. This becomes of great importance should formwork be removed too soon where the reliance on models established for PC systems may no longer be suitable. Under such conditions, hydration will be very much incomplete, with previous research indicating minor or no reaction of PFA over the first 7 days (Fraay et al., 1989, Deschner et al, 2012) and only slightly faster reaction rates for GGBS (Escalante et al, 2001). In both cases the result will be an underdeveloped and exposed microstructure, possibly susceptible to ingress from aggressive species.

Furthermore, the reduced $Ca(OH)_2$ content, characteristic of composite cement materials, presents additional limitations when considering resistance to carbonation induced corrosion. The decrease in portlandite content, the main alkalinity buffer within hardened cement paste, results in a reduced pH. This allows carbonation to occur at elevated rates and to greater extents; behaviour likely to become more pronounced with increasing levels of replacement. Moreover, the expected retardation of the rate of CO_2 ingress typically observed in PC systems is a result of densification of the microstructure. This, however, is not concurrent with the behaviour exhibited in composite cements with high replacement levels, which are adversely affected by a coarser microstructure and a greater porosity.

This project has examined the early stage carbonation behaviour of immature low-clinker binders, focusing on the effects that insufficient curing and phase carbonation have on the phase assemblage composition and the development of the microstructure. The work will attempt to examine differences between these systems and conventional studies on mature systems.

2. Experimental

2.1. Materials

A CEM I 52.5R cement was selected for this study in order to improve early age strength development in the composite systems. The chemical composition, determined by x-ray fluorescence (XRF), for the CEM I 52.5R, PFA and GGBS used are shown in Table 1. Table 2 displays the mineralogical composition of the cement clinker.

Table 1. Chemical composition of raw materials

		LOI	SiO_2	Al_2O_3	Fe_2O_3	TiO_2	MnO	CaO	MgO	SO_3	K_2O	Na_2O	P_2O_5	Total
CEM I 52.5R	%	1.50	20.50	4.60	2.40	0.30	0.00	63.40	2.00	3.60	0.74	0.13	0.30	99.47
PFA	%		70.83	24.36	2.24	1.48	0.05	0.06	0.23	0.00	0.64	0.10	0.05	100.04
GGBS	%	2.35	35.71	10.65	0.45	0.73	0.23	43.32	3.97	3.06	0.45	0.16	0.02	98.74

Table 2. Mineralogical composition of CEM I 52.5R

		C_3S	C_2S	C_3A	C_4AF
CEM 52.5R	%	68	10	9	7

2.2. Method

Four paste systems (CEMI, and CEMI with replacement by 30% PFA, 30% & 60% GGBS) at a w/b ratio of 0.57 were investigated. The CEM I 52.5R used was free from limestone, and replacement in the composite systems was by volume. Following preliminary testing, and to mimic procedures which did not deviate too greatly from those used in practice, a curing duration (t_0) of 72 hours was selected. This duration allowed the systems to develop enough strength to allow sample preparation and conditioning to be performed, while still representing the short curing period typically employed in practice.

Samples were cast and sealed in small plastic vials (ø = 12 mm, h = 47 mm) and rotated for 72 hours in a temperature controlled laboratory (22° +/-2°C) before being cut to a thickness of 0.5 mm and subjected to conditioning at either ambient CO_2 conditions (300-400 ppm CO_2, approx. 24°C) or in a CO_2 free environment. All samples were conditioned at a relative humidity (RH) of 72.6% for up to 14 days. Characterisation was performed on the samples at t_0, 1, 2, 4, 7 & 14 days.

In order to study the effects of carbonation on the phase assemblage and microstructure only, very thin samples (0.5mm) were used, allowing the impact on the reaction kinetics to be investigated separately from effects on both the porosity and the transport properties. Although the porosity and the transport properties are important factors on the effects, and rate, of carbonation, the results here focus on the changes in the phase assemblage and microstructure when there is no influence from porosity.

Simultaneous thermal analysis (STA) was collected using a Stanton Redcroft Simultaneous Thermal Analyser STA 780 under a nitrogen atmosphere, heating from 20°C to 1100°C at a rate of 10°C/min. STA was used to quantify the amount of precipitated $Ca(OH)_2$ and $CaCO_3$ in the samples, as well as the bound water content. A selection of samples were also analysed by thermogravimetric (TG) analysis coupled with Fourier transform infrared (FTIR) spectroscopy in order to identify the gases evolved and improve accuracy of results, this was performed using a Stanton Redcroft TGH1000 paired with a Thermo Scientific Nicolet Is10 spectrometer. Attenuated total reflectance FTIR (ATR-FTIR) spectroscopy data was collected using a Thermo Scientific Nicolet Is10 spectrometer, fitted with a Thermo Scientific Smart Diamond ATR sampling accessory over a wave number range of 0 - 4000cm^{-1}. Raman spectroscopy measurements were performed using a Horiba Jobin Yvon HR 800 LabRAM instrument (Villeneuve d'Ascq, France) equipped with an Olympus BX40 microscope (focus graduation 1 µm), a He-Ne laser working at 633 nm and a multi-channel air-cooled CCD detector, the Raman shift was calibrated against the 520 cm^{-1} peak of silicon. Spectra were acquired between 100 – 1200 cm^{-1} and 3000 – 4000 cm^{-1} and data handling was performed using OPUS spectroscopy software. X-ray diffraction (XRD) patterns were collected with a Bruker D2 Phaser equipped with CuKα radiation source between 5 – 70° 2θ, a step size of 0.008 and a dwell time of 1.0 second were used. Analytical transmission electron microscopy (TEM) data was collected on Ar ion-beam milled samples using a FEI Tecnai F20 200 kV FEG TEM fitted with a Gatan Orius SC600 CCD camera and an Oxford Instruments 80mm2 SDD EDX detector running INCA software.

Organic solvent exchange was used to halt hydration in the samples prior to analysis. The samples were immersed in isopropanol for a period of 2 hours and then washed with diethyl ether (washing repeated 3 times) and finally heated at 40°C on a hotplate for 10 minutes. Isopropanol has been shown to be the most effective selection for solvent exchange for young cement samples, causing minimal damage to the phases and microstructure (Zhang & Scherer, 2011).

3. Results and Discussion
3.1. Characterisation of phase assemblage
ATR-FTIR data were collected for all samples exposed to ambient CO_2. Figure 1 displays the characteristic ATR-FTIR absorbance band for carbonates between 1400 - 1500cm^{-1} collected for the 30% PFA system. Exposure to CO_2 led to an increase in $CaCO_3$ content. Furthermore a sizeable

increase in carbonate content was observed between 2 and 4 days CO_2 exposure. Considering the normalised spectra for the silicate band and the $Ca(OH)_2$ peak (Figure 2(a)), this considerable increase in carbonate content coincides with both the complete consumption of $Ca(OH)_2$, as demonstrated in Figure 2(b), and the decalcification of C-S-H, demonstrated by a shift in the silicate band to slightly higher wavenumbers (Figure 2(a). This loss of buffering capacity allows carbonation to progress much more rapidly within the sample, and it appears that carbonation of C-S-H begins only once there is no more $Ca(OH)_2$ available.

Similar behaviour was observed for all samples, but at different lengths of exposure. For the CEMI system this occurred between 4 and 7 days, then between 2 and 4 days for the 30% GGBS system and 1-2 days for the 60% GGBS system. The lower initial $Ca(OH)_2$ content in the composite blends resulted in a loss of buffering capacity at an earlier age compared with CEMI systems, behaviour exacerbated with increasing levels of replacement.
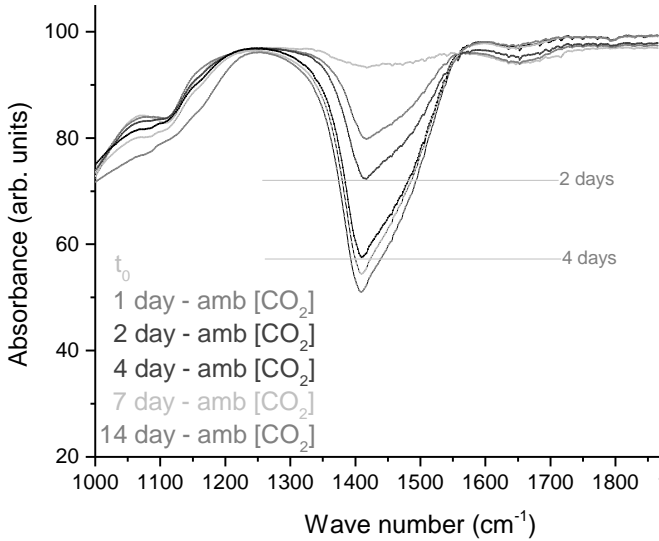

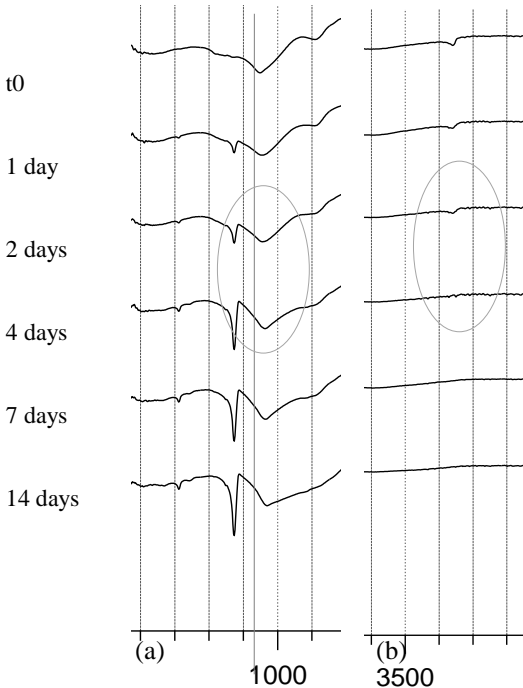Figure 1. ATR-FTIR spectra for 30% PFA showing $CaCO_3$ content between $1000 – 1800 cm^{-1}$

Figure 2. ATR-FTIR spectra showing (a) silicate bands and (b) $Ca(OH)_2$ peak ($3643 cm^{-1}$)

Figure 3 displays the $Ca(OH)_2$ (2(a)) and $CaCO_3$ (2(b)) contents, as calculated from the STA data. A large increase in carbonate content was seen with the entire, or almost nearly entire, consumption of $Ca(OH)_2$, consistent with the ATR-FTIR data. Furthermore, faster, more extensive carbonation was observed for both composite systems at 30% replacement compared to the CEMI sample. This reflects the lower portlandite content, underlining the need for prolonged curing. Composite materials, with slower rates of hydration, subjected to curing lengths of only a few days will exhibit open and underdeveloped microstructures, in which carbonation rate will occur much more rapidly. This difference in behaviour, between 'idealised'/28 day lab cured samples and a more realistic curing length, emphasises the need for updated carbonation models and approaches.
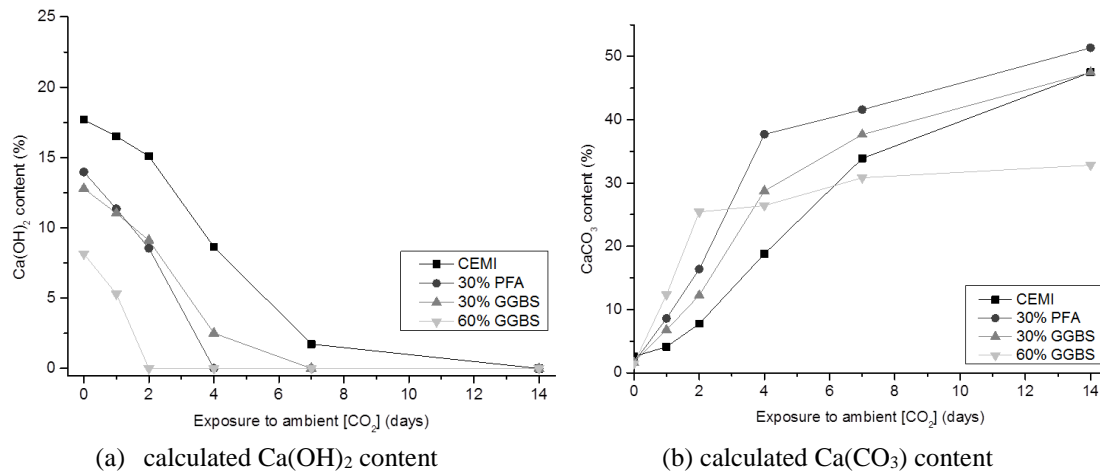

(a) calculated $Ca(OH)_2$ content
(b) calculated $Ca(CO_3)$ content

Figure 3. Key phase composition as determined from TGA data for samples exposed to ambient $[CO_2]$

Furthermore the extent of carbonation was affected by both the replacement material and level. Although similar carbonation behaviour was observed for the materials with equal replacement levels, carbonation occurred to a greater degree, and at a faster rate, for the PFA system compared with the GGBS system. This is a reflection of the PFA's slower reaction rate, Lam et al measured the degree of hydration of a PC paste, with w/b ratio 0.5, to be 65% following 7 days curing, while the degree of hydration of the fly ash in a PC paste with 25% replacement by PFA was just 6.4% at the same age (Lam et al 2000). The adverse effects of a slower hydration rate on carbonation resistance are expected to be magnified with decreasing curing length. Carbonation was initially much faster in the 60% GGBS sample, with a vast increase in carbonate content between t_0 and 2 days (Figure 3(b)), however a plateau was reached at 4 days, with minimal subsequent carbonation, data supported by the ATR-FTIR data. This suggests that, with the limited degree of hydration likely in a high replacement system at an early age, all potential carbonatable hydration phases have been carbonated by this time.

STA and ATR-FTIR data showed that the samples conditioned in a CO_2 free environment underwent no continued hydration at 72.6% RH. This is in agreement with the findings of Ho et al who demonstrated that there is minimal hydration at RH levels below 80% (Ho et al 1989).

In addition to quantifying the degree of carbonation, thermal analysis could also shed light on the nature of the carbonate species formed. There are typically 3 decomposition modes associated with carbonation (Thiery et al 2007); mode I ($780^{\circ} - 990^{\circ}C$), mode II ($680^{\circ} - 780^{\circ}C$) and mode III ($550^{\circ} - 680^{\circ}C$). The higher decomposition modes, mode I & II, are attributed to crystalline polymorphs of $CaCO_3$ (calcite, vaterite and aragonite), with mode I being principally attributed to calcite. Mode III is believed to be associated with amorphous $CaCO_3$.

As carbonation progressed, and the measurable level of carbonates increased, the mass loss associated with $CaCO_3$ dropped to a lower temperature (Table 3). This behaviour coincided with both the loss of $Ca(OH)_2$ and the significant increase in carbonate content as previously indicated by the ATR-FTIR and TGA data. This strongly indicated carbonation via decalcification of C-S-H, further corroborating

the shift in silicate bands observed in the infrared spectra. It is considered that the carbonation of C-S-H corresponded to the formation of poorly crystallised and metastable forms of $CaCO_3$.

Table 3. Temperature at which mass loss due to $CaCO_3$ decomposition begins

	Temperature CaCO3 decomposition begins (oC)					
	Ages (days)					
	t0	1 day	2 days	4 days	7 days	14 days
CEMI	550	560	550	530	**455**	400
30% PFA	550	540	530	**410**	400	400
30% GGBS	580	540	530	**450**	450	390
60% GGBS	550	520	**310**	350	300	230

This behaviour was further reinforced when the carbonation of a CH free C-S-H sample was considered. Figure 4 displays the TGA plots of a synthesised C-S-H sample (free from CH and with a Ca/Si 1.33), before and after carbonation. The sample was carbonated under the same conditions as the cement samples in this study for a period of four days. The carbonates produced as a result of carbonation of C-S-H decompose at a much lower temperature than those from CH carbonation. The decomposition temperature here is in fact lower than the three decomposition modes typically considered for $CaCO_3$ and indicate the formation of an amorphous calcium carbonate.
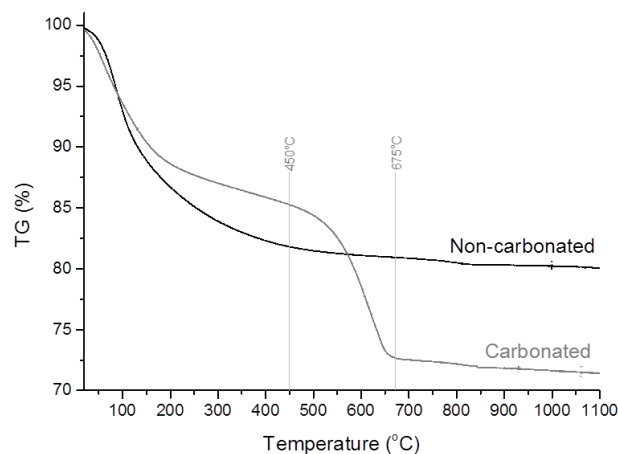

Figure 4. TGA plot from a synthetic C-S-H (Ca/Si ratio 1.33) before and after carbonation (24ºC, 72.6% RH, ambient [CO_2], exposure time – 4 days)

Villain et al (2007) suggested that, for highly hydrated (cured for 3 months) mortar samples subjected to accelerated carbonation, the dissociation of stable $CaCO_3$ (calcite), attributed to $Ca(OH)_2$ carbonation, occurred between $650º – 950ºC$, while unstable forms of vaterite and aragonite resulting from C-S-H carbonation dissociated between $530º – 650ºC$. Accelerated carbonation has been extensively researched, reporting the simultaneous carbonation of $Ca(OH)_2$ and C-S-H, with a much faster carbonation rate of $Ca(OH)_2$ initially observed, the rate decreasing as carbonate phases were produced at the crystal surface (Groves et al 1991, Thiery et al 2007). The results presented here indicate modifications in the carbonation mechanism between accelerated and natural carbonation, as well as between mature and immature specimens. Moreover, carbonation at ambient CO_2 concentrations for samples cured for 72 hours implies that it is the $Ca(OH)_2$ phase initially involved in the carbonation reaction, and once consumed, then carbonation of C-S-H begins.

TG-FTIR was performed on selected samples in order to correctly identify the mass loss associated with bound water and that associated with $CaCO_3$. The mass loss associated with carbonates began at lower temperatures, than conventionally established, in many of the samples (Table 3). Figure 5

displays a TG-FTIR plot for the 30% GGBS sample exposed to ambient CO_2 for 4 days, and verifies the mass loss due to $CaCO_3$ began at 450ºC. In this sample a small amount of portlandite was also present (Figure 3(a)), however the FTIR data for H_2O and CO_2 confirm that the mass loss below 450ºC can be attributed predominantly to bound water, including mass loss associated with CH, and above this temperature the mass loss was clearly a result of carbonate species. Although a minor mass loss above 450ºC was detected for H_2O, this was only slight and observed in all the systems. TG-FTIR analysis was performed on the samples in which a drop in $CaCO_3$ decomposition temperature had been observed but there was also portlandite present, the results were consistent, supporting previous observations and assumptions. This had a subsequent effect on the calculation of the bound water content, lowering the uppermost temperature value (typically 500/550ºC) to avoid overlap with the mass loss attributed to $CaCO_3$.
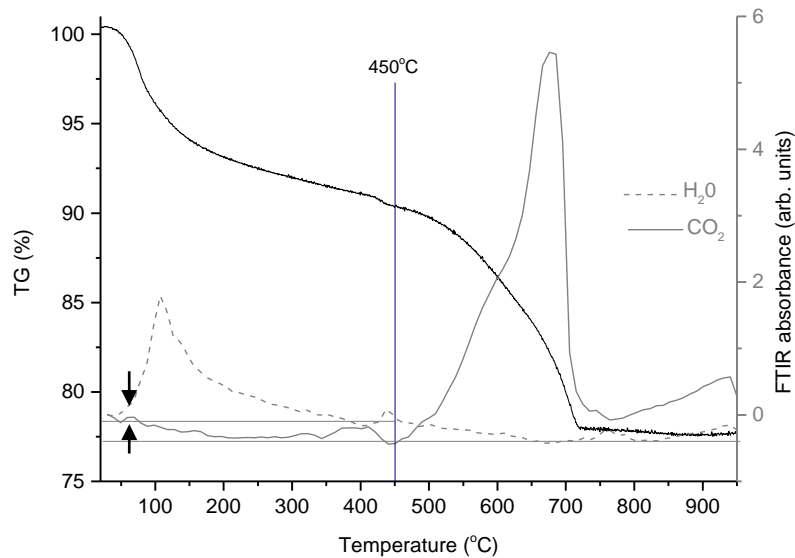

Figure 5. TG-FTIR plots for 30% GGBS – exposed to ambient [CO_2] for 4 days.
FTIR spectra shown for H_2O and CO_2.

Raman spectroscopy and XRD analysis were in very good agreement with one another. Both analysis techniques predominantly detected calcite as the $CaCO_3$ polymorph formed due to carbonation, however vaterite was also observed in small amounts in the PFA system. Figure 6 displays the Raman spectra for the PFA samples between t_0-7 days exposure to CO_2. The spectra are presented over the range 100-1200cm^{-1}. The absence of the characteristic band due to portlandite at 359 cm^{-1} in the carbonated samples further confirmed its complete consumption at the same ages as indicated in both the ATR-FTIR and STA data. What was unclear was the presence of an amorphous $CaCO_3$ phase. The strongest (v_1) bands for of calcite and amorphous $CaCO_3$ are at 1085cm^{-1} and 1077cm^{-1} respectively, if both are present, as expected once decalcification of C-S-H has begun, it is not obvious whether both would be easily differentiated. It is possible that calcite is much more dominant, and therefore much more clearly observed, as many studies in which amorphous $CaCO_3$ has been reported, detect the amorphous polymorph only when the crystalline ones are not present (Black et al 2007, Dubina et al 2013).
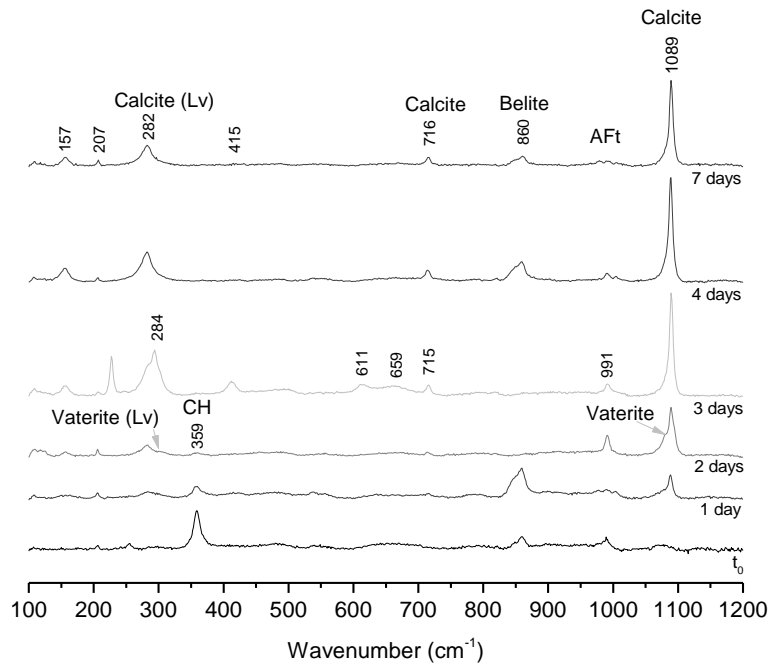
Figure 6. Raman spectroscopy spectra for 30% PFA exposed to ambient [CO_2] for t_0-7 days

TEM-energy dispersive x-ray (EDX) analyses of both inner product (Ip) and outer product (Op) C-S-H were collected for the 30% GGBS and 30% PFA systems following exposure for 4 days. All areas were checked to be free from crystalline phases by selected area electron diffraction (SAED) before analysis. The mean Ca/Si, Ca/(Al+Si) and Al/Si ratios for Ip and Op C-S-H are given in Table 4 for the slag sample for both the non-carbonated (4(a)) and carbonated (4(b)) systems.

The non-carbonated sample showed a Ca/Si ratio of 1.39 and an Al/Si ratio of 0.16 (Op) and 0.11 (Ip). It has been well established in the literature that a decrease in the Ca/Si ratio of C-S-H is observed with increasing levels of replacement by GGBS (Richardson & Groves, 1992; Taylor et al 2010). The Ca/Si ratio of C-S-H in PC systems is typically ≈1.7-1.8 (Richardson, 2000), while Richardson and Groves (1993) reported Ca/Si ratios of 1.69 and 1.65 for Op and Ip C-S-H, respectively, in a one week old OPC paste. The Ca/Si ratios in Table 4(a) therefore indicate notable reaction of the GGBS at this age, correlating well with ratios reported for similar levels of replacement in other studies. For example Taylor et al (2010) observed a Ca/Si ratio of 1.56 for Op C-S-H and 1.50 for Ip C-S-H with an average Al/Si ratio of 0.09 in a 25% GBBS paste sample.

Table 4. Mean Ca/Si, Ca/(Al+Si) and Al/Si ratios for C-S-H for 30% GGBS

(a) conditioned for 4 days at 0% [CO_2]

	N	Ca/Si Mean	Ca/Si S.D.	Ca/(Al+Si) Mean	Ca/(Al+Si) S.D.	Al/Si Mean	Al/Si S.D.
Op	50	1.48	0.18	1.28	0.12	0.16	0.07
Ip	25	1.22	0.08	-	-	0.11*	-
All	75	1.39	0.20				

(b) conditioned for 4 days at ambient [CO_2]

	N	Ca/Si Mean	Ca/Si S.D.	Ca/(Al+Si) Mean	Ca/(Al+Si) S.D.	Al/Si Mean	Al/Si S.D.
Op	15	0.60	0.07	0.55	0.06	0.10	0.03
Ip	33	0.53	0.06	-	-		-
All	35	0.57	0.07				

N = number of analyses, S.D. = standard deviation

*Determined from regression analysis of Al/Si – Mg/Si plots at Mg/Si = 0

Figure 7 shows a plot of Al/Si versus Mg/Si for the Ip analyses in the non-carbonated and carbonated 30% slag samples. The Mg/Al ratio of the hydrotalcite-like phase is derived from the gradient of the linear regression line and was shown to be 2.78 for the sample conditioned free from CO_2. Although many studies observe a much lower value for cement systems, of approximately 2, the samples studied here are very early age, and the Mg/Al ratio is expected to decrease with time (Taylor et al., 2010).
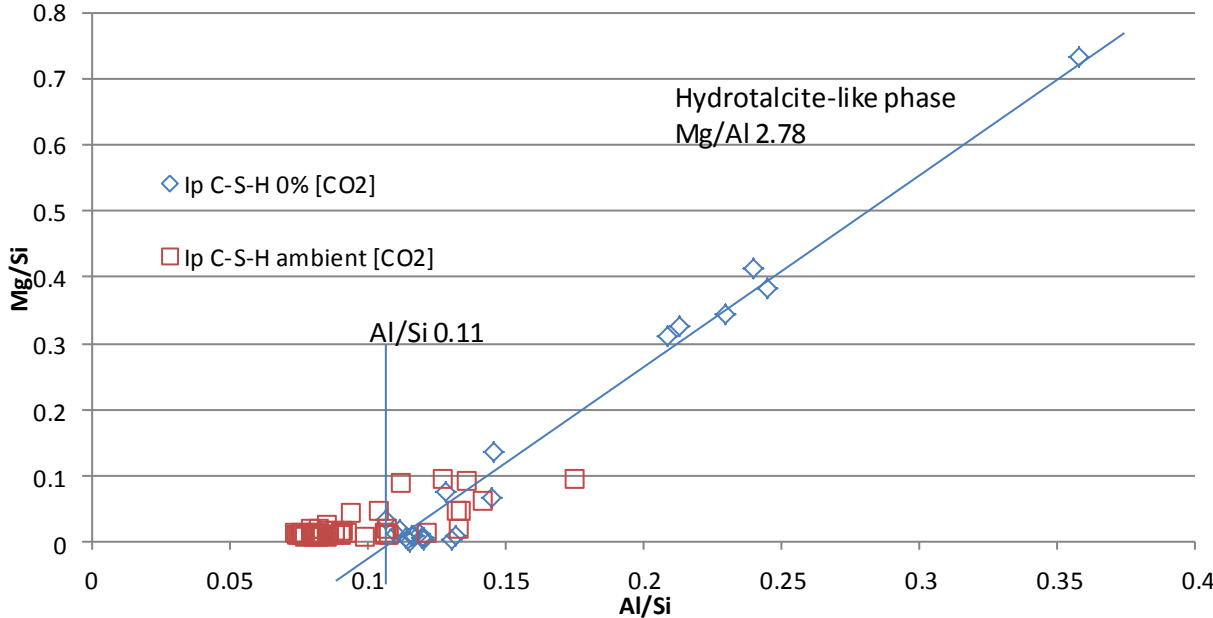

Figure 7. Al/Si – Mg/Si plots of TEM-EDX data collected from Ip regions for 30% GGBS

The Ca/Si ratios in Table 4(b) for the carbonated slag sample confirms that decalcification of C-S-H had begun at this age, supporting previous observations for the carbonation of C-S-H in both the ATR-FTIR and STA data. If the level of carbonation is then considered, in terms of the change in Ca/Si ratio before and after carbonation, it appears that a similar level of decalcification had occurred in both the Ip (% carbonation = 56.6%) and Op (% carbonation = 59.5%) C-S-H. In addition to the decalcification of the C-S-H, the EDX analyses also showed an accompanying decrease in the Al/Si ratio of the Op regions, indicating the removal of aluminium from the C-(A)-S-H phase. However, in order to accurately calculate the Al/Si ratio of the Ip C-S-H and Mg/Al ratio of the hydrotalcite-like phase for the carbonated sample, more EDX data points are required.

Table 5. Mean Ca/Si, Ca/(Al+Si) and Al/Si ratios for C-S-H for 30% PFA conditioned for 4 days at 0% [CO_2]

		Ca/Si		Ca/(Al+Si)		Al/Si	
	N	Mean	S.D.	Mean	S.D.	Mean	S.D.
Op	25	1.62	0.10	1.37	0.09	0.13	0.05
Ip	19	1.53	0.08	-	-	-	-
All	44	1.55	0.10				

EDX data was also collected for the 30% PFA system, following exposure to a CO_2 free environment for 4 days, the results are displayed in Table 5. The higher Ca/Si ratio compared to the GGBS system was immediately apparent. Both Fraay et al. (1989) and Deschner et al. (2012), reported minimal or no measurable reaction of PFA in composite cements, up to an age of 7 days. It was therefore expected that at this early age the PFA will have undergone minimal reaction at most; as was reflected in the EDX data obtained. The Ca/Si ratios indicate that it was predominantly hydration of the cement grains that had occurred, although the ratios were lower than anticipated for a neat PC system, as discussed

previously, potentially suggesting slight reaction of the fly ash. This slower reaction rate was also inferred in the ATR-FTIR and STA data which showed a greater, and faster rate, of carbonation in comparison to the 30% GGBS samples. A faster carbonation rate indicates a porous, less developed, microstructure in which CO_2 is able to diffuse through the material more easily. This is further highlighted when related to Ca/Si ratios reported in the literature, for example Girao et al. (2010) measured Ca/Si ratios of 1.49 and 1.41 for Op and Ip C-S-H respectively in a 30% PFA system at an age of one month. Al/Si ratios of 0.15 for Op regions and 0.17 for Ip regions were also observed. It is expected that longer curing will cause a decrease in the Ca/Si ratio and an increase in the Al/Si ratio.
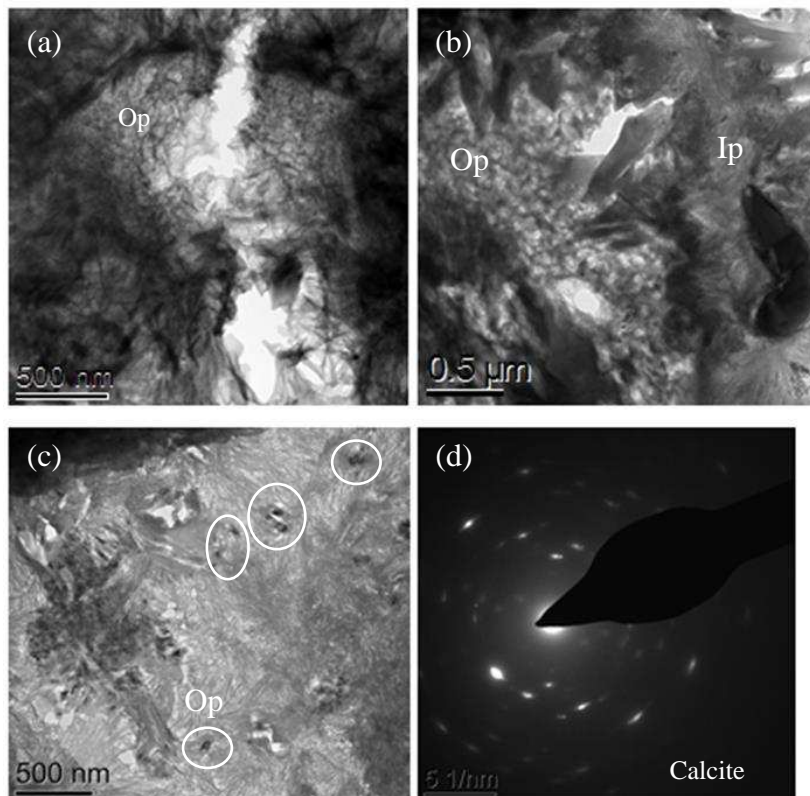
3.2 Microstructural Characterisation

Figure 8. TEM micrographs for 30% GGBS sample after 4 days exposure at (a) 0% CO_2 (b) ambient CO_2 (c) ambient CO_2 (d) SAED pattern for crystals in (c), SAED pattern

Figure 8 displays TEM micrographs from the 30% GGBS sample after exposure to CO_2 free (a) and ambient CO_2 ((b)&(c)) environments for 4 days. Both fibrillar and foil like Op C-S-H, characteristic of PC-GGBS materials, is clear in the images, with some fine Ip C-S-H also present in 8(b). The images clearly highlight the effects of carbonation on the Op regions. The carbonated sample shows a coarsening of the Op C-S-H, compared to the non-carbonated sample, further reinforcing decalcification of C-S-H at this age (Groves et al 1991). Figure 8(b) indicates that there was no change in the Ip region, this was observed in all the micrographs recorded. Figure 8(c) displays microcrystals of calcite that had formed on the fibrils of Op C-S-H, confirmed to be calcite by SAED pattern (Figure 8(d)). However no microcrystals of $CaCO_3$ were observed in any of the Ip regions of the carbonated sample. This suggests that the Ip region is unaffected by carbonation, whereas the EDX analysis clearly demonstrates a decrease in the Ca/Si ratio of the Ip C-S-H as a result of carbonation. A similar decrease in terms of decalcification is in fact observed for the Ip and Op regions. Groves et al (1990), proposed that the decrease in the Ca/Si ratio of the Ip C-S-H without any visual change in the microstructure was the cause of carbonation shrinkage; the Ca^{2+} cations migrating from Ip regions to

Op regions in order to maintain equilibrium due to a concentration gradient. The absence of microcrystals in the Ip phase suggests this theory.

Similar behaviour was also observed in the 30% PFA systems, Figure 9 shows micrographs from the 30% PFA system for both non-carbonated (a) and carbonated (b) samples. Coarsening of the Op C-S-H following carbonation was evident, while the Ip regions appeared unaltered, and microcrystals of $CaCO_3$ had formed on the Op fibrils only. It is interesting to note the foil-like morphology of the Op C-S-H in both images ((a)&(b)), indicating that there has been some reaction of the PFA, the foil like nature of the phase suggests a lowering of the Ca/Si ratio (Richardson & Groves, 1992). Figure 9(c) shows an enlargement of the PFA particle in the bottom right of the micrograph in 9(a), in which a very slight reaction rim is evident. This demonstrates that the PFA has undergone a minor reaction, which is also supported by the lower Ca/Si ratio, when compared to typical PC samples, determined in the EDX data. This evidence supports the reaction of the PFA following only 72 hours curing, notably earlier than in other studies (Fraay et al, 1989, Deschner et al, 2012).
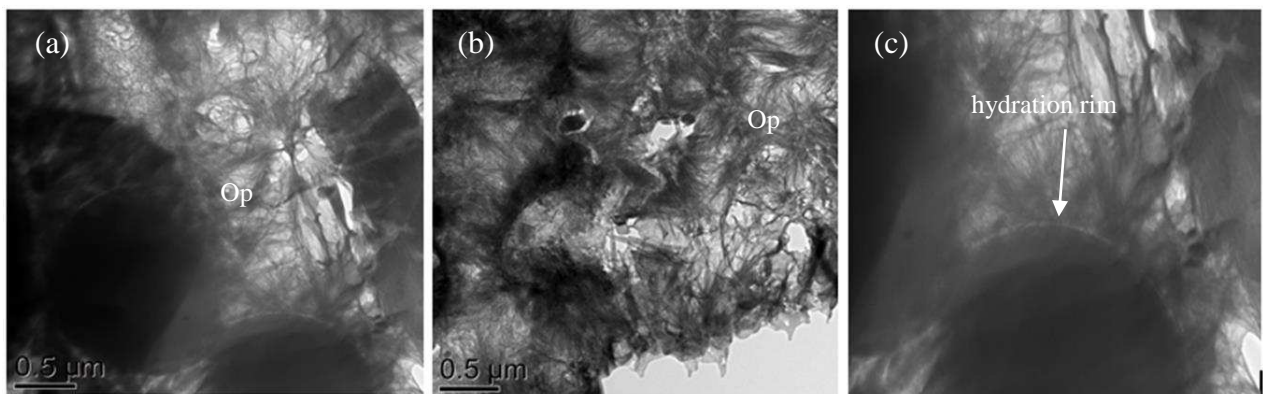

Figure 9. TEM micrographs for 30% PFA sample after 4 days exposure (a) 0% CO_2 (b) ambient CO_2
(c) enlargement of PFA particle in Figure 7(a)

4. Conclusions

Carbonation of immature paste samples was followed by a range of characterisation techniques. There was no continued hydration and changes were due to carbonation only. CEMI systems showed better carbonation resistance, in terms of the phase assemblage composition, compared to composite systems following curing for 72 hours. More extensive carbonation was evident in the composite systems, behaviour attributed to a more porous material with a less developed microstructure. A notable increase in carbonation was observed as $Ca(OH)_2$ was completely consumed, the loss of buffering capacity allowing carbonation to occur more rapidly. This coincided with C-S-H decalcification, confirmed by ATR-FTIR, TGA & TEM data. This occurred at an earlier age with increasing levels of replacement, believed to be a result of the already initially lower $Ca(OH)_2$ content, typical of composite cement materials. STA data showed that as carbonation continued, a drop in $CaCO_3$ decomposition temperature was observed, coinciding with the consumption of $Ca(OH)_2$. This lower temperature also indicated formation of poorly crystalline or amorphous $CaCO_3$ due to carbonation of C-S-H. Carbonation of $Ca(OH)_2$ and C-S-H did not occur simultaneously, decalcification of C-S-H only beginning once $Ca(OH)_2$ had been consumed. Raman and XRD analysis both identified calcite as the polymorph chiefly formed from carbonation, with some vaterite also produced in the PFA samples. TEM-EDX data for the 30% GGBS system gave comparable Ca/Si ratios to those reported in the literature. The Mg/Al ratio of the hydrotalcite-like phase was higher than typically observed in cement systems, however this is expected to decrease with age. Following 4 days exposure to CO_2, a notable decrease in the Ca/Si ratio of both the Ip and Op C-S-H was evident. Decalcification of the C-S-H was also accompanied by dealumination of the Op region. Ca/Si and Al/Si ratios for the non-carbonated 30% PFA sample indicated only very minor reaction of the PFA had occurred following 72 hours curing. TEM micrographs for the 30% GGBS and 30% PFA show coarsening of the OP C-S-H

following carbonation, however the Ip regions appeared to be unaffected. Microcrystals of $CaCO_3$ were observed in Op areas only, forming on Op C-S-H fibrils, suggesting the decrease in the Ca/Si ratio of the Ip C-S-H is as a result of the migration of Ca^{2+} cations driven by a concentration gradient.

Acknowledgements

References

- Black L., et al, 2007. Structural features of C-S-H(I) and its carbonation in air – a Raman spectroscopic study. Part II: Carbonated phases. Journal of the American Cermaic Society, 90, 908-917.
- Çakır Ö., Aköz F., 2008.Effect of curing conditions on the mortars with and without GGBFS. Construction and Building Materials, 22, 308-314.
- Deschner F., et al, 2012. Hydration of Portland cement with high replacement by siliceous fly ash. Cement and Concrete Research, 42, 1389-1400.
- Dubina E., et al, 2013. Influence of water vapour and carbon dioxide on free lime during storage at 80ºC, studied by Raman spectroscopy. Spectrochimia Acta Part A. Molecular and Biomolecular Spectroscopy, 111, 299-303.
- Escalante J. I., et al, 2001. Reactivity of blast-furnace slag in Portland cement blendshydrated uner different conditions. Cement and Concrete Research, 31, 1403-1409.
- Fraay, A. L. A., et al, 1989. The reaction of fly ash in concrete. A critical examination. Cement and Concrete Research, 19, 235-246.
- Girao A. V., et al, 2010. Composition, morphology and nanostructure of C-S-H in 70% white Portland cement – 30% fly ash blends hydrated at 55ºC. Cement and Concrete Research, 40, 1350-1359.
- Groves G. W., et al, 1991. Progressive changes in the structure of hardened C_3S cement pastes due to carbonation. Journal of the American Ceramic Society, 74, 2891-2896.
- Groves G. W., et al 1990. The carbonation of hardened cement pastes. Advances in Cement Research, 3, 117-125.
- Ho D. W. S., et al, 1989. The influence of humidity and curing time on the quality of concrete. Cement and Concrete Research, 19, 457-464.
- Lam L., et al, 2000. Degree of hydration and gel/space ratio of high-volume fly ash/cement systems. Cement and Concrete Research, 30, 747-756.
- Poon C. S., et al, 1997. The influence of different curing conditions on the pore structure and related properties of fly-ash cement pastes and mortars. Construction and Building Materials. 11, 383-393.
- Richardson I. G., Groves G. W., 1992. Microstructure and microanalysis of hardened cement pastes involving ground granulated blast-furnace slag. Journal of Materials Science, 27, 6204-6212.
- Richardson I. G., Groves G. W., 1993. Microstructure and microanalysis of hardened ordinary Portland cement pastes. Journal of Materials Science, 28, 265-277.
- Richardson I. G., 2000. The nature of the hydration products in hardened cement pastes. Cement and Concrete Composites, 22, 97-113.
- Taylor R., et al 2010. Composition and microstructure of 20-year-old ordinary Portland cement-ground granulated blast furnace slag blends containing 0-100% slag. Cement and Concrete Research, 40, 971-983.
- Thiery M., et al, 2007. Investigation of the carbonation front shape on cementitious materials: Effects of the chemical kinetics. Cement and Concrete Research, 37, 1047-1058.
- Villain G., et al, 2007. Measurement methods of carbonation profiles in concrete: Thermogravimetry, chemical analysis and gammadensimetry. Cement and Concrete Research, 37, 1182-1192.
- Zhang J., Scherer G. W., 2011. Comparison of methods for arresting hydration of cement. Cement and Concrete Research, 41, 1024-1036.